LBNL-41076
UC-401
Preprint

ERNEST ORLANDO LAWRENCE BERKELEY NATIONAL LABORATORY

Crossed Beam Reaction of $O(^1D) + D_2 \rightarrow OD + D$ by Velocity Map Imaging: The Role of Excited States

Musahid Ahmed, Darcy S. Peterka, and Arthur G. Suits

Chemical Sciences Division

November 1997

Submitted to
Journal of Chemical Physics

REFERENCE COPY
Does Not
Circulate

Bldg. 50 Library - Ref.
Lawrence Berkeley National Laboratory

LBNL-41076
Copy 1

DISCLAIMER

This document was prepared as an account of work sponsored by the United States Government. While this document is believed to contain correct information, neither the United States Government nor any agency thereof, nor the Regents of the University of California, nor any of their employees, makes any warranty, express or implied, or assumes any legal responsibility for the accuracy, completeness, or usefulness of any information, apparatus, product, or process disclosed, or represents that its use would not infringe privately owned rights. Reference herein to any specific commercial product, process, or service by its trade name, trademark, manufacturer, or otherwise, does not necessarily constitute or imply its endorsement, recommendation, or favoring by the United States Government or any agency thereof, or the Regents of the University of California. The views and opinions of authors expressed herein do not necessarily state or reflect those of the United States Government or any agency thereof or the Regents of the University of California.

LBNL-41076
UC-401

Crossed Beam Reaction of $O(^1D) + D_2 \rightarrow OD + D$ by Velocity Map Imaging: The Role of Excited States

Musahid Ahmed, Darcy S. Peterka, and Arthur G. Suits

Chemical Dynamics Group
Chemical Sciences Division
Ernest Orlando Lawrence Berkeley National Laboratory
University of California
Berkeley, California 94720

November 1997

This work was supported by the Director, Office of Energy Research, Office of Basic Energy Sciences, Chemical Sciences Division, of the U.S. Department of Energy under Contract No. DE-AC03-76SF00098.

Crossed Beam reaction of $O(^1D) + D_2 \rightarrow OD + D$ by Velocity Map Imaging: The Role of Excited States.

Musahid Ahmed, Darcy S. Peterka and Arthur G. Suits

Chemical Dynamics Group

Chemical Sciences Division

Ernest Orlando Lawrence Berkeley National Laboratory

Berkeley, CA 94720

Abstract

The technique of velocity map imaging [A. T. J. B. Eppink, and D. H. Parker, Rev. Sci. Instrum. 68, 3477 (1997)] has been applied to the reaction $O(^1D) + D_2 \rightarrow OD + D$ under single collision conditions in crossed molecular beams at collision energies (E_{coll}) of 2.8 and 5.5 kcal/mol. Images of the reactively scattered D atom product were recorded, yielding the full double differential cross sections (energy and angle) for the reaction. The observed D atom angular distribution is broad in the backward sphere and sharply peaked in the forward sphere, and the translational energy release and angular distributions are strongly coupled. There is an increase in scattering in the backward sphere with an increase in collision energy. Although the overall translational energy distributions do not change significantly with E_{coll} we observe an increase in the contribution in the backscattering at the higher E_{coll}. These observations are ascribed to the interplay of the ground state potential energy surface (1A') with excited states (1A", 2A') which can lead to different scattering mechanisms (insertion versus abstraction) as has been suggested recently in theoretical and experimental studies.

Introduction

The reaction $O(^1D)$ with molecular hydrogen and its isotopic variants has long been considered a prototypical insertion reaction, with most collisions at thermal energies believed to access the region of the deep H_2O well[1] . An early crossed molecular beam study found forward-backward symmetry in the angular distribution for collision at 2.7 kcal/mol[2]. This was ascribed to an insertion reaction mechanism, with symmetry in the decaying intermediate invoked to account for the angular distribution. Rotational distributions of the product OH for the first few vibrational levels have been shown to be broad and strongly inverted using laser induced fluorescence (LIF) methods[3-4]. LIF measurements of the OH vibrational distribution find that it is slightly more excited than expected on statistical grounds[5], whereas chemical laser gain[6] and chemiluminescence experiments[7-8] suggest that it is even more excited than the LIF results, indicating direct dynamics. Trajectory calculations[9-13] and a quantum reactive scattering study with reduced dimensionality[14] have, in the past, consistently shown forward-backward symmetric angular distributions and thus the importance of the insertion mechanism. Recent work, both theoretical and experimental, has begun to challenge this notion of simple insertion on the ground electronic potential energy surface (PES).

Che and Liu, using a conventional Doppler-shift technique in conjunction with crossed molecular beams, observed enhanced back scattering for collisions of $O(^1D)$ with HD at 4.55 kcal/mol[15]. Hsu and Liu confirmed this observation very recently using a high resolution Doppler-selected time-of-flight method[16]. They were also able to see some structure in the energy distributions at different angles which they believed correlated to vibrational-rotational states of the corresponding OH/OD product. Casavecchia[17] and coworkers at Perugia and Miau[18] at Berkeley also reported asymmetry in the angular distributions for a range of collision energies. Subsequently Ho *et al.* carried out trajectory calculations based on a new global potential energy surface[19]. Their results

support the insertion mechanism with a short-lived complex, and they could not reproduce the strong preference for backward scattering seen in the work of Che and Liu. Alexander *et al.* have also performed QCT calculations on the $O(^1D)$ + HD reaction[20]. Their results agreed with the translational energy distributions ($P(E_T)$'s) extracted from Che and Liu's earlier experiment, but their state averaged angular distribution showed forward-backward symmetry. Alexander *et al.* also studied the $O(^1D) + H_2$ reaction using polarized Doppler resolved laser spectroscopy to probe the product state resolved differential cross section under bulb conditions[21]. They found strongly peaked backward scattering in the channel generating OH (v'=0, N=5) but their collision energy was not well defined.

Peng *et al.* reported a time-dependent three-dimensional quantum dynamics study for this reaction[22]. Despite the presence of the deep well, no long-lived resonances were found in their calculations. Their results also support the insertion mechanism for this reaction. Dai has recently performed an exact quantum state-to-state dynamics calculation[23], and showed that there is a strong dependence on energy (6.9-18.5 kcal/mol) for the state-to-state reaction probabilities while the total reaction probability has a clear plateau in the high-energy region. He inferred that the reaction was direct when the collision energy is not too low, but identified several resonances in the low-energy region.

All though there are five PESs accessible at thermal energies, the theoretical calculations mentioned above have used a single valued PES. Kuntz *et al.* were the first to explore the role of excited states in this reaction[24-26]. They performed a multi surface QCT study of the dynamics of this reaction using the diatomics-in-molecules approach to generate the excited surface. On the ground state surface they found the insertion mechanism dominant, but trajectories run on the first excited surface showed marked asymmetry in angular distributions. There was a dominance of scattering in the backward direction with strong dependence on collision energy, suggesting that an abstraction type

mechanism comes into play with the inclusion of the first excited state surface. However, their 3.7 kcal/mol barrier to this collinear approach implied a minimal importance for this mechanism under thermal conditions.

Hsu *et al.* measured the dependence of the integral cross-sections for the $O(^1D)$ + D_2 (H_2, HD) reaction on collision energies[27]. They found the cross-sections decreased rapidly with collision-energy, leveled off at about 2 kcal/mol, and then slowly increased again. This behavior was explained by invoking two reaction pathways: an insertion type mechanism at lower collision energies, and an abstraction mechanism at the higher energies. They also suggest that the abstraction pathway comes into play when the reactants access the first excited potential energy surface. Schatz *et al.* have developed a global potential energy surface for the first excited (1A") surface of H_2O, which they have incorporated in extensive QCT calculations[28]. Their results showed a growing contribution for excited state reaction at energies above the barrier. One very important observation in this paper was that even though the excited state reactive cross-section was only a small fraction of the total cross-section, it did populate very specific product vibrational states (v'=3-4) and gives strongly backward peaked differential cross-sections. Based on these theoretical calculations and the recent molecular beam studies, it is now clear that excited electronic states must play some role in this reaction at collision energies above about 2 kcal/mol.

We have begun an in-depth experimental study to explore the role of excited states using the ion imaging technique in crossed molecular beams. Ion imaging is a multiplexing method which provides simultaneous detection of all recoil velocities, both speed and angle, for the detected product. One of the most appealing factors is the very direct way the raw data presents itself to the experimenter. Further, the images may be directly deconvoluted to yield the velocity-flux contour maps which summarize the dynamics. The deconvolution does not require the simplifying assumption of uncoupled translational energy and angular distributions usually employed in analyzing reactive

scattering experiments. The imaging experiments thus directly reveal the genuine double differential cross sections ($d^2\sigma/dE_T d(\cos\theta)$), a particularly important feature in the $O(^1D)$ + D_2 reaction.

To date, there have been two scattering experiments performed with traditional ion imaging techniques- inelastic scattering of Ar-NO[29] and reactive scattering[30] of H + D_2. In the past, the ion imaging technique has suffered from limited velocity and angular resolution, determined by the dimensions of the interaction region relative to the detector, transmission reduction, and by blurring from lensing effects associated with the grids. A recent advance by Eppink and Parker[31] involves simply replacing the conventional grids of the Wiley-McLaren time-of-flight (TOF) spectrometer with open electrostatic lenses and adjusting the potentials to achieve momentum focusing. Under these conditions, termed "velocity map imaging", all products with the same initial velocity vector in the plane parallel to the detector are focused to the same point, irrespective of their initial distance from the ion lens axis. The ability to focus images gives rise to "deblurring" and results in a vast improvement in experimental resolution, limited in our experiments by the velocity spread of the beams. A similar technique has been used in conjunction with "recoil-ion momentum spectroscopy" in the field of atomic and molecular physics for some time[32]. This technique is being used to determine the charge state and complete final momemtum vector of a recoiling target ion emerging from an ionizing collision of an atom with any kind of radiation.

Experimental

The crossed molecular beams apparatus (Fig. 1) has been described in detail in a recent publication[33]. The $O(^1D)$ beam was generated by photolyzing O_3 seeded in He, using the 266 nm output of a Nd-YAG laser (Spectra-Physics GCR 290-30), at the nozzle of a Proch-Trickl piezoelectric pulsed valve[34]. The molecular beam of ozone was generated by passing helium through ozone trapped on silica gel, held at -40° C. After the

beam was collimated by a skimmer, it was chopped by means of a rotating slotted wheel (200 Hz, dia: width:1 mm), to generate a short rectangular pulse (7.5 μs) of $O(^1D)$. The oxygen atom beam velocity and spread were monitored using either (2+1) REMPI of $O(^1D)$ or, conveniently, vacuum-ultraviolet (VUV) photoionization of the O_2 co-photo fragment (using the same light used to probe the reactively scattered D atom product). By changing the photolysis laser delay relative to the chopper and probe laser, the velocity of the oxygen beam could be changed between 1650 and 2250 m/s. Neat D_2 was expanded through another Prock-Trickl pulsed valve, collimated by a single skimmer and the beams were allowed to interact on the axis of the velocity focusing time-of-flight mass spectrometer. The speed of the D_2 beam could be increased by heating the nozzle source. We could generate velocities up to 4000 m/s using this heated source.

The resultant D atom was ionized using a two color (1+1) (λ = 121.6 and 212.5 nm) REMPI scheme. The VUV Lyman-α light was generated by difference frequency mixing[35] of ultraviolet (UV) and infrared (IR) light in krypton, phase matched with argon. The UV light (212.5 nm) was generated by doubling the output of a seeded Nd-Yag (Spectra-Physics GCR 290-30) pumped dye laser (Laser Analytical Systems LDL) operating at 637.5 nm in β- barium borate (BBO), then mixing the resultant UV light with the dye fundamental in a second BBO crystal. Infrared light around 840 nm was generated using a second Nd-Yag pumped dye laser (Laser Analytical Systems LDL), and the two beams were collimated using a dichroic mirror and focused into the rare gas cell. The resultant VUV output was loosely focused into the interaction region of the molecular beams using a MgF_2 lens.

The D^+ ion was accelerated toward a 40-mm diameter dual multichannel plate (MCP) (Galileo 3040FM) coupled to a fast phosphor screen and imaged on a fast scan charge-coupled device camera with integrating video recorder (Data Design AC-101M). The gain was adjusted in conjunction with a binary video look-up table allowing us to integrate single ion hits on the MCP. Images were accumulated while scanning across the

Doppler profile of the D atom, since the line width of the laser light was narrower than the Doppler spread. The recorded image is actually a 2-dimensional (2-D) projection of the nascent 3-dimensional (3-D) velocity distribution, but established tomographic techniques enable us to reconstruct the 3-D distribution[36]. Typical accumulation time for a single collision energy was about 120 minutes. A background image obtained with the photolyis laser off was subtracted from the data image, but this represented a minor correction.

Fig. 2 shows the advantage of using velocity mapping techniques. Shown are images of background D atoms and O_2 in the molecular beam. The upper image was generated using the conventional ion-imaging technique, the lower image with velocity map imaging. The stripe on the upper image and the large circle in the lower image are background D atoms generated from D_2 dissociation on a hot filament ion gauge. The O_2 is the photofragment co-product from O_3 dissociation at 266 nm entrained in the molecular beam. The O_2 image spread and displacement from the center of the images in the lower figure reflects the speed ratio and angular divergence of that species in the molecular beam. In the case of the D atom image, comparing Fig. 2 A to Fig. 2 B, we see that the background laser stripe which was formed by ionizing D atoms in the laser path has collapsed to a circle. This circle represents the normal room temperature Boltzmann distribution of the D atoms in the vaccuum chamber. As is apparent from these two images, velocity mapping has deblurred the image and also dramatically improved the resolution in our experiment.

Results

We have studied the reaction over a range of collision energies. Images recorded for the D atom reactively scattered product at 5.5 kcal/mol and 2.8 kcal/mol are shown in Fig. 3 A and B , respectively. The velocity of $O(^1D)$ was 1800 m/s (speed ratio ~10) for both collision energies, while it was 2000 m/s (speed ratio ~10) for D_2 at 2.8 kcal/mol

and 3400 m/s (speed ratio ~5) at 5.5 kcal/mol. The relative velocity vector is vertical in the plane of the figure, with the center-of-mass velocities of the reactant beams indicated. The dominant feature, apparent at both collision energies, is the broader and faster backscattering of the D atom relative to the incoming D_2 beam and the sharper peaking distribution in the forward direction. This gives rise to an overall "arrowhead" shape to the distribution and gives us an indication about the scattering dynamics for this reaction. The cylindrical symmetry of the experiment justifies the use of the inverse Abel transform method to reconstruct the full 3D distributions.

We have extracted differential cross sections for these two collision energies. The c.m. angular distributions [$d\sigma/d(\theta)$], extracted from the images are shown in Fig. 4. A and B respectively. At 2.8 kcal/mol, the 0° distribution is 80% and the 90° distribution is 30% compared to the 180° distribution. In addition there is a hump in the distribution between 120 to 160° giving rise to a much broader backward distribution as is already apparent in the raw data. At 5.5 kcal/mol, the forward scattering peak has been further attenuated and now we have 60% compared to the backward scattering, the 90° distribution is essentially the same. Also at 5.5 kcal/mol we see the hump between 120-160°. Previous published angular distributions showed forward-backward symmetry at a collision energy of 2.7 kcal/mol, for the $O + H_2$ system[2]. Very recent experimental results from other groups[15-18] show that there is marked asymmetry in the angular distributions with predominance in the backward direction as the collision energy is increased beyond 2 kcal/mol. We have compared our scattering angular distributions at 2.8 kcal/mol with recent theoretical results for 2.7 kcal/mol, for $O + H_2$ from Schatz. *et al.* [28]. These are shown in fig 4 B.

A revealing way to look at the detailed dynamics of this system is to display the angular distributions for different segments of the translational energy distributions. Fig. 5 show the angular distributions for 8 regions of the translational energy distributions for both E_{coll} = 2.8 and 5.5 kcal/mol. The angular distributions are similar within

experimental error at both collision energies, but there is a distinctive rise in the backward scattering for translational energy distributions from 8.6 to 26.3 kcal/mol.

Fig. 6 and 7 shows the translational energy distributions obtained from the Abel transformed image for 9 distinct regions of angular recoil (from 0° to 180°, in 20° increments). At E_{coll} = 2.8 kcal/mol, the forward component peaks at lower translational energy, ~ 5.5 kcal/mol, but tails off beyond 33 kcal/mol, while the backward portion peaks at about ~ 11 kcal/mol and drops sharply beyond 27.5 kcal/mol. The sideways component peaks at about ~ 8.3 kcal/mol, but then drops sharply beyond 16.5 kcal/mol. At E_{coll} = 5.5 kcal/mol, the results are similar for the forward and sideways scattered components, but there is a distinctive shift to more translational energy release in the backward sphere. The filled area in Fig. 6 and 7 shows the difference in translational energy release at the two collision energies. The data have been normalised to each other taking into account the increase in the reaction cross-section at 5.5 kcal/mol[27]. The O + D_2 reaction is exoergic by 43.9 kcal/mol, hence we do not expect dramatic changes in the translational energy release with a slight change in collision energy. We do see an enhancement in translational energy release in the backward sphere especially in the 100°-160° region. This correlates to the hump that we see in the angular distributions.

Discussion

The $O(^1D)$ atom can interact with both deuterium atoms or with only one of them depending on the direction of approach. The first case is characterized as the lateral attacking or insertion process, and as the reactants approach each other the potential energy surface manifold splits into five surfaces (3 singlet and 2 triplet). A schematic of the potential energy surfaces is shown in fig. 8. If the approach is in the C_{2v} configuration, the reaction intermediate is directly correlated with the $^1A_1$ ground state of the water molecule (or $^1A'$ in C_s symmetry). This part of the surface is purely attractive.

In the second case, where the oxygen atom interacts with only one D atom, if the approach is exactly collinear ($C_{\infty v}$), the system is degenerate[37], resulting in three surfaces ($^1\Sigma^+$, $^1\Pi$, $^1\Delta$). The $^1\Delta$ surface is purely repulsive, the $^1\Pi$ state rises up in energy compared to the initial reactants and the $^1\Sigma^+$ state is slightly lower in energy. However, the ground state of OH is a $^2\Pi$ state while the excited state is a $^2\Sigma^+$ state. This means that the two surfaces must cross somewhere on the reaction coordinate. As states of different symmetry do not interact, the two surfaces merely intersect on their way to the products. At energies below the threshold for formation of electronically excited OD($^2\Sigma^+$), collinear reaction is not possible and the likely result is elastic or inelastic scattering.

If the geometry of the nuclei is changed slightly, the point group defining the system changes from $C_{\infty v}$ to C_s, and the PES's change in symmetry. The $^1\Sigma^+$ state becomes the $1A'$ surface, while the degeneracy of the $^1\Pi$ state is removed, splitting into the $2A'$ and $1A''$ surfaces. The two A' surfaces, being of the same symmetry type, can now interact. Whereas in the collinear geometry there is a surface crossing, at near collinear geometries the two surfaces are coupled and an avoided crossing occurs. This is a conical intersection. One can imagine looking at these surfaces as the O-D-D bond angle changes from bent to straight to bent. The surfaces are apart, repelling one another, as one approaches 180°, the surfaces get closer, till at exactly 180° they touch, at a single point. The region of the conical intersection is schematically shown in Fig. 9 roughly based on recent calculations by Dobbyn and Knowles[38]. Reactants approaching on the ground $1A'$ surface may proceed adiabatically to products, skirting the cone, so long as the angle γ is sufficiently far from 180°. For geometries near collinear, the 1A' and 2A' surfaces interact strongly, and nonadiabatic transitions may occur between them. However, for strictly collinear geometries, the reaction must proceed 'diabatically' as states of different symmetry species are not coupled. Hence there should be a decrease in the direct backscattered distribution for trajectories on the ground potential energy

surface, in effect yielding a "shadow" of the conical intersection. This decrease may be somewhat offset by reaction that proceeds on the excited state surfaces. These correlate directly to ground state products and any collisions on the 2 A' and 1 A" surfaces should be reactive in character.

As mentioned in the introduction, classical and quasiclassical trajectory studies show that most of the reactions proceed through the insertion geometry because of the deep potential minimum and the absence of a potential barrier in the entrance channel. This frequently occurs even if the initial approach is collinear[25]. This is because the hydrogen molecule is so light that it can respond to any change in the PES almost adiabatically and reorient itself so eventually the oxygen atom will be at the lateral position. The water complex that is formed may sample the potential well several times, undergoing bending motion before decomposing into products. The complex will therefore have time to redistribute its energy among different degrees of freedom and trajectory calculations[11,12] show a monotonic distribution in the vibrational state distribution of the OH product. However product state distribution experiments have consistently shown that the vibrational distributions are inverted. Hence, a insertion pathway to explain the vibrational distributions is clearly inadequate. There have also been some trajectory calculations[12,25] which show that, if the reactants go through the minimum once or not at all, the mechanism is direct abstraction giving rise to inverted vibrational distributions. This inversion increases with collision energy and gives us an indication that the redistribution of the excess energy among different degrees of freedom is not complete.

The story is completely different when the excited states are invoked. Since there is a significant barrier when the oxygen atom attacks the hydrogen molecule laterally on the first excited surface we will only consider the collinear approach. Reactions starting on this surface for non-linear geometries must go through the avoided crossing and cross back to the ground adiabatic surface before reaction can occur as shown in Fig. 9.

Trajectory calculations[25,26] show that for collinear geometries, the most reactive encounters go directly to products, only a small portion falls back into the deep potential energy well. The calculations[26] also suggest that some of the reactions on this surface will go through migration, so the oxygen atom actually reacts with the second hydrogen atom instead of the first one it encounters. For the direct abstraction reactions, the OH products possess an excess amount of vibrational energy and show an inverted vibrational distribution. At the same time, the OH products are strongly backscattered with respect to the incoming oxygen atoms. The fact that we see a broad peak in the backward scattered direction in the OD product distribution also agrees with the theoretical prediction that the avoided crossing of the two adiabatic surfaces is energetically accessible within a large range of O-D-D bond angles.

Schatz *et al.*[28] have quantified the contribution of the 1A" excited state on the title reaction. Trajectory calculations show that the signature for the excited states is enhanced backscattering in the angular distributions as expected for rebound dynamics, and very specific populations of low rotational levels of the v' = 3 and 4 vibrational states of the OH fragment. Furthermore they argue that the 2A' surface also makes an important contribution to the vibrational and angular distributions at high energies. Two key results from our experiments are - (1) enhanced backscattering with an increase in collision energy and (2) this backscattering is associated with a translational energy release that correlates with low N rotational, v'=3 and 4 vibrational distributions of OD as shown in Fig. 7. This agrees very well with the recent theoretical predictions.

Hsu *et al.*[27] have measured the branching between the insertion and abstraction mechanisms from integral cross section measurements. Their results for $O(^1D) + D_2$ show that at E_{coll} = 2.8 kcal/mol, abstraction contributes only about 5% to the total reaction cross-section, but at E_{coll} = 5.5 kcal/mol, the contribution rises to around 20%. These results are also closely borne out by the QCT calculations carried out by Schatz *et al.*[28] invoking participation of the excited states. If we integrate the differential cross section

for translational energy release between 8.6 - 26.3 kcal/mol, and compare them at the two collision energies in our experiment, we get an increase of ~25% with an increase in E_{coll}. If we postulate that this increase is due to the abstraction channel, this agrees well with the integral cross-section measurements.

Furthermore, if we plot the difference in translational energy release for the two collision energies we can isolate the excited state contribution for this reaction. This is only possible because of the unique dynamics in this system, in which the ground state translational energy release is relatively insensitive to collision energy and the large difference, shown by the filled area in fig. 6 and 7, is clearly due to the contribution of the excited states. Also shown in fig. 7 are the positions for various rotational levels for v' = 3 and 4 vibrational distributions for the corresponding OD. We see a substantial contribution precisely where the low N, v'=3,4 distribution is expected to appear as predicted by Schatz *et al.*[28].

Finally we are encouraged with the fit of the QCT calculations of Schatz *et al.*[28] with our experimental results at 2.8 kcal/mol as shown in fig. 4 B. The fit in the backward sphere is not good using the single 1A' PES but with inclusion of the first excited state 1A" the fit is excellent. Our results show that even at relatively low collision energies, the first excited state plays a important part in this reaction. The contribution of this excited state is increased with an increase in collision energy as is seen with the rise of the backscattering component of the differential cross-section at 5.5 kcal/mol. There could also be other subtle mechanisms in operation here. There is considerable opportunity for interaction between the 1A" and 2A' surfaces in the entrance channel. In addition, the collinear reaction represents a likely occasion for quantum mechanical interference between flux on the various surfaces, yielding possible oscillations in the angular distributions and a clear potential role for the geometric phase. We do see oscillations in the experimental angular distributions but our signal to noise ratio is not good enough for us to make any substantive claims. Further theoretical studies will be necesary to

investigate these phenomena in detail and to provide experimentalists with a yard stick to observe such quantum phenomenon.

Conclusion

The $O(^1D) + D_2 \rightarrow OD + D$ reaction has been examined under single collision conditions in crossed molecular beams at collision energies of 2.8 and 5.5 kcal/mol using velocity map imaging. Backward scattering is enhanced with an increase in collision energy. Energy-dependent trends in the differential cross-sections show that excited states play an important role in this reaction as recently postulated by Schatz *et al.*[28] and also invoked by Hsu *et al.*[27] to interpret their integral cross-section measurements for this reaction. The excited states contribute to an abstraction type mechanism which leads to enhanced backward scattering and populations of low N, v'=3 and 4 distributions for the OD molecules as seen in these experiments.

Acknowledgements

The authors gratefully acknowledge G. Schatz, K. Liu, and P. Cassavechia for valuable discusssions and comments, and K . Liu, G. Schatz, D. Parker, P. Casavechia and P. J. Knowles for providing preprints of their most recent work. AGS would like to thank D. Chandler and the Sandia Combustion Research Facility for hosting a recent workshop on imaging methods at which the velocity mapping technique was discussed. This work was supported by the Director, Office of Energy Research, Office of Basic Energy Sciences, Chemical Sciences Division of the U. S. Department of Energy under contract No. DEACO3-76SF00098.

References

1. R. D. Levine and R. B. Bernstein, *Molecular Reaction Dynamics and Chemical Reactivity* (Oxford University, New York, 1987).

2. R. J. Buss, P. Casavecchia, T. Hirooka, S. J. Sibener, and Y. T. Lee, Chem. Phys. Lett. 82, 386 (1981).

3. A. C. Luntz, R. Schinke, W. A. Lester, Jr., and Hs. H. Grunthard, J. Chem. Phys. 84, 5365 (1986).

4. J. E. Butler, G. M. Jursich, I. A. Watson, and J. R. Wiesenfeld, J. Chem. Phys. 84, 5365 (1986).

5. G. M. Jursich and J. R. Wiesenfeld, Chem. Phys. Lett. 119, 511 (1985).

6. Y. Huang, Y. Gu, C. Liu, X. Yang, and Y. Tao, Chem. Phys. Lett. 127, 432 (1986).

7. J. E. Butler, R. G. McDonald, D. J. Donaldson, and J. J. Sloan, Chem. Phys. Lett. 95, 183 (1983).

8. P. M. Aker and J. J. Sloan, J. Chem. Phys. 85, 1412 (1986).

9. K. S. Sorbie and J. N. Murell, Mol. Phys. 31, 905 (1976).

10. R. Schinke and W. A. Lester, Jr., J. Chem. Phys. 72, 3754 (1980).

11. S. W. Ransome and J. S. Wright, J. Chem. Phys. 77, 6346 (1982).

12. P. A. Whitlock, J. T. Muckerman, and E. R. Fisher, J. Chem. Phys. 76, 4468 (1982).

13. L. J. Dunne and J. N. Murell, Mol. Phys. 50, 635 (1983).

14. J. K. Badenhoop, H. Koizumi, and G. C. Schatz, J. Chem. Phys. 91, 142 (1989).

15. D. -C. Che and K. Liu, J. Chem. Phys. 103, 5164 (1995).

16. Y. T. Hsu, and K. Liu, J. Chem. Phys. 107, 1664 (1997).

17. M. Alagia, N. Balucani, L. Cartechini, P. Casavecchia, E. H. van Kleef, G. G. Volpi, P. J. Kuntz, and J. J. Sloan, (to be published).

18. T. T. Miau, PhD thesis, University of California, Berkeley (1995).

19. T. -S. Ho, T. Hollebeek, H. Rabitz, L. B. Harding, and G. C. Schatz, J. Chem. Phys. 105, 10472 (1996).

20. A. J. Alexander, F. J. Aoiz, M. Brouard, and J. P. Simons, Chem. Phys. Lett. 256, 561 (1996).

21. A. J. Alexander, F. J. Aoiz, M. Brouard, I. Burak, Y. Fujimura, J. Short, and J. P. Simons, Chem. Phys. Lett. 262, 589 (1996).

22. T. Peng, D. H. Zhang, J. Z. H. Zhang, and R. Schinke, Chem. Phys. Lett. 248, 37 (1996).

23. J. Dai, J. Chem. Phys. 107, 4934 (1997).

24. P. J. Kuntz, B. I. Niefer, and J. J. Sloan, J. Chem. Phys. 88, 3629 (1988).

25. P. J. Kuntz, B. I. Niefer, and J. J. Sloan, Chem. Phys. 151, 77 (1991).

26. P. A. Berg, J. J. Sloan, and P. J. Kuntz, J. Chem. Phys. 95, 8038 (1991).

27. Y. T. Hsu, J. -H. Wang and K. Liu, J. Chem. Phys. 107, 2351 (1997).

28. G. C. Schatz, A. Papaioannou, L. Pederson, L. B. Harding, T. Hollebeek, T. -S. Ho, and H. Rabitz, J. Chem. Phys. 107, 2340 (1997).

29. A. G. Suits, L. J. Bontuyan, P. L. Houston, and B. J. Whitaker, J. Chem. Phys. 96, 8618 (1992).

30. T. A. Kitsopoulos, D. P. Baldwin, M. A. Buntine, R. N. Zare, and D. W. Chandler, Science. 260, 1605 (1993).

31. A. T. J. B. Eppink, and D. H. Parker, Rev. Sci. Instrum. 68, 3477 (1997).

32. V. Frohne, PhD thesis, Kansas State University (1994); V. Mergel, R. Dorner, J. Ullrich, O. Jagutzki, S. Lencinas, S. Nuttgens, L. Spielberger, M. Unverzagt, C. L. Cocke, R. E. Olson, M. Schulz, U. Buck, E. Zanger, W. Theisinger, M. Isser, S. Geis, and H. Schmidt-Bocking, Phys. Rev. Lett. 74, 2200 (1995); J. Ullrich, R. Moshammer, R. Dorner, O Jagutzki, V Mergel, H. Schmidt-Bocking, and L. Spielberger, J. Phys. B: At. Mol. Opt. Phys. 30, 2917 (1997).

33. M. Ahmed, D. Blunt, D. Chen, and A. G. Suits, J. Chem. Phys. 106, 7617 (1997).

34. D. Proch and T. Trickl, Rev. Sci. Instrum. 60, 713 (1989).

35. G. Hilber, A. Lago, and R. Wallenstein, J. Opt. Soc. Am. B. 4, 1753 (1987).

36. B. J. Whitaker, in *Research in Chemical Kinetics Vol. 1*, edited by R. G. Compton and G. Hancock (Elsevier, Amsterdam, 1993).

37. S. P. Walch and L. B. Harding, J. Chem. Phys. 88, 7653 (1988).

38. A. Dobbyn and P. J. Knowles, Mol. Phys. 91, 1107 (1997).

Figure Captions

FIG. 1. Schematic view of the experimental setup.

FIG. 2. Images of background D atoms and O_2 molecular beam. The upper image (A) was generated using the conventional ion-imaging technique, the lower image (B) with velocity map imaging. The stripe on the upper image and the circle in the lower image are D atoms generated from D_2 dissociation on a hot filament ion gauge. The O_2 is the photofragment co-product from O_3 dissociation at 266 nm.

FIG. 3. (A) Image of D atoms formed in the reaction of $O(^1D) + D_2$ at a collision energy of 5.5 kcal/mol using velocity map imaging. The arrows show the relative velocities of the beams in the center-of-mass frame. The short arrow corresponds to the $O(^1D)$ beam while the long arrow corresponds to the D_2 beam. (B) Same as (A) but collision energy is 2.8 kcal/mol.

FIG. 4. (A) Center-of-mass angular distributions obtained from the Abel-transformed image for $E_{coll} = 5.5$ kcal/mol . The direction of the D_2 and $O(^1D)$ beams correspond to 0^0 and 180^0, respectively. (B) Same as (A) but $E_{coll} = 2.8$ kcal/mol. The thin line is experimental data; the thick line is QCT calculations by Schatz *et al.*[28] using a single (1A') PES and the dotted line is QCT calculations[28] including contribution from the 1A" PES performed on the $O(^1D) + H_2$ reaction at $E_{coll} = 2.7$ kcal/mol.

FIG. 5. Center-of-mass angular distributions obtained for a range of translational energy release. The solid line represents data for E_{coll} = 2.8 kcal/mol, the dashed line for E_{coll} = 5.5 kcal/mol.

FIG. 6. Translational energy distributions obtained from Abel-transformed images for distinct regions of angular recoil. The solid line represents data for E_{coll} = 2.8 kcal/mol, the dashed line for E_{coll} = 5.5 kcal/mol. The filled area is the difference in translational energy release for the two collision energies.

FIG. 7. Translational energy distributions obtained from Abel-transformed images for 160°-180° angular recoil. The solid line represents data for E_{coll} = 2.8 kcal/mol, the dashed line for E_{coll} = 5.5 kcal/mol. The filled area is the difference in translational energy release for the two collision energies. (+) and (l) represent different rotational levels for the corresponding vibrational levels of OD taking into account momentum and energy conservation.

FIG. 8. Semiquantative singlet state correlation diagram for the reaction $O(^1D) + D_2 \rightarrow OD + D$.

FIG. 9. Illustration of the region of the conical intersection. The range of γ is $180^{o} \pm 5^{0}$. The region of increasing OD-D distance leading to products is to the left of the figure. The labels Σ and Π refer to the centerline of the surfaces, for γ=180°.

Fig-1. AHMED et al.

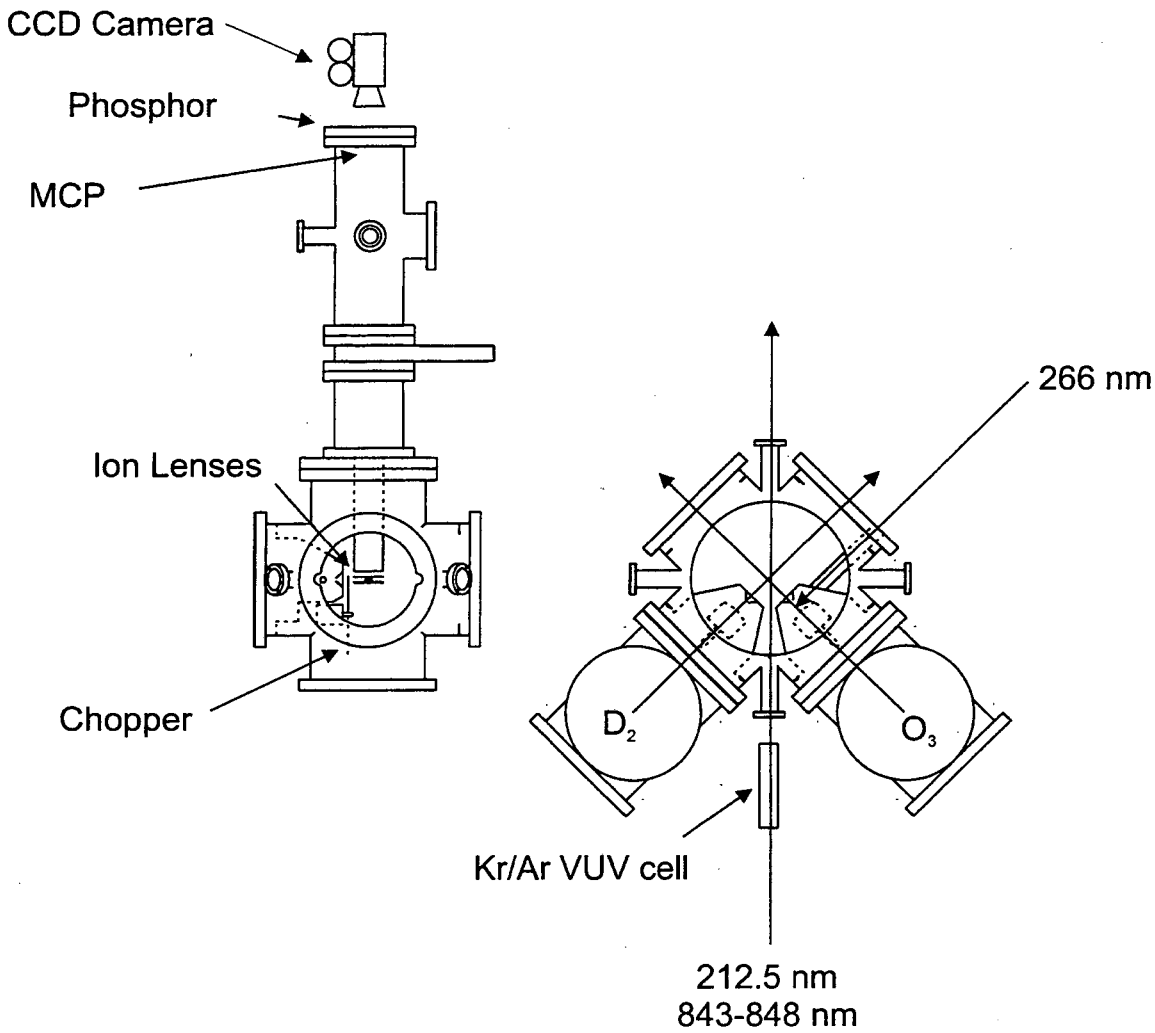

Fig. 2. AHMED et al.

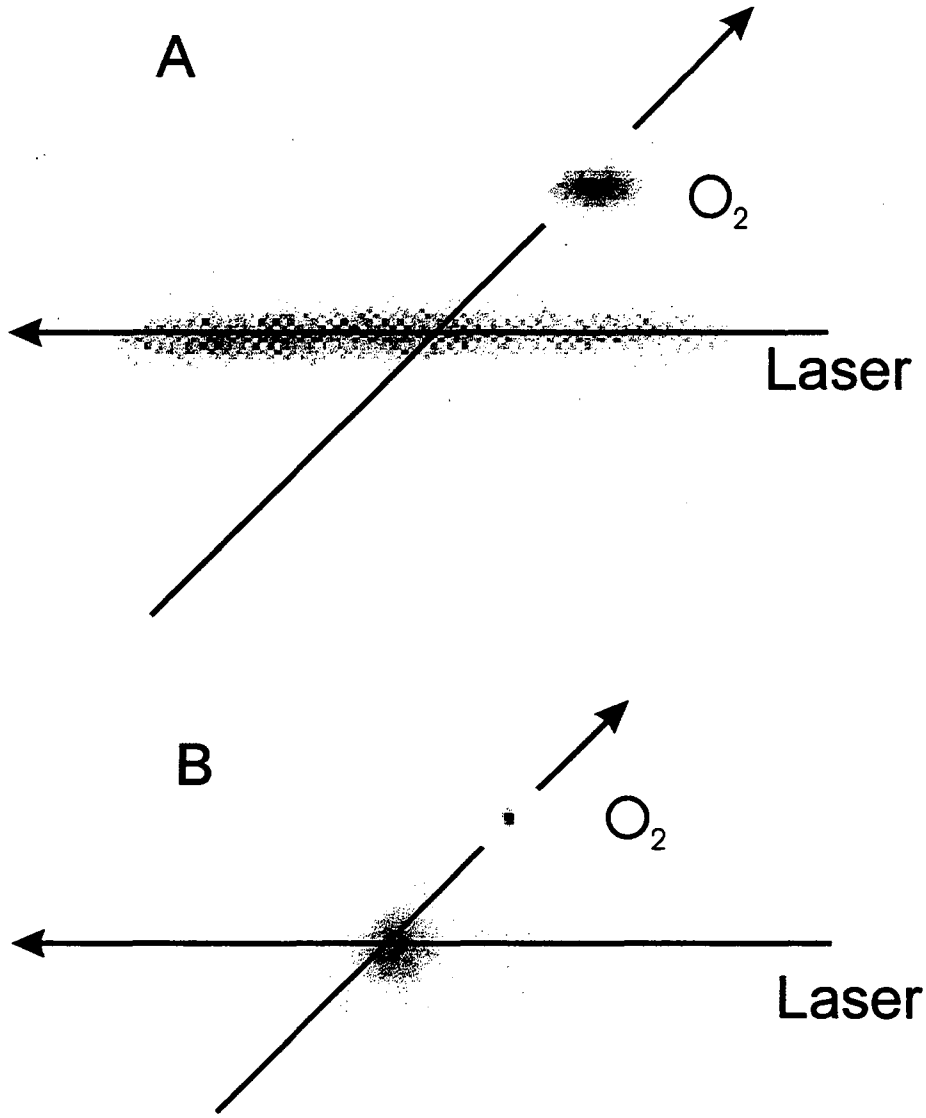

A

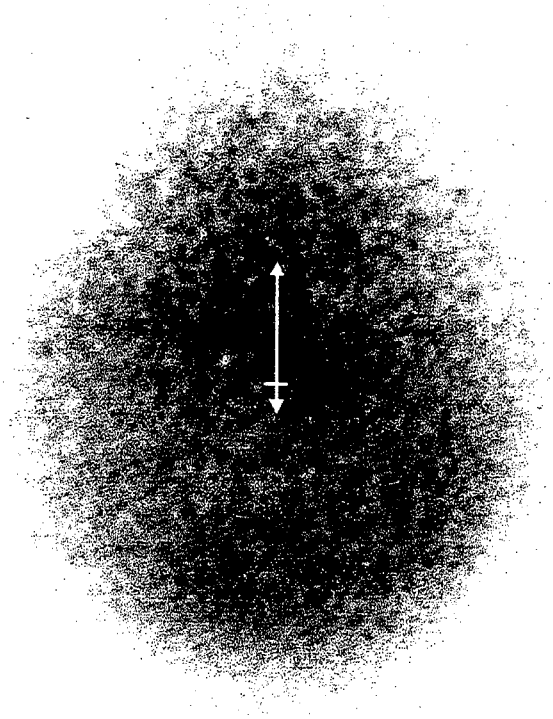

B

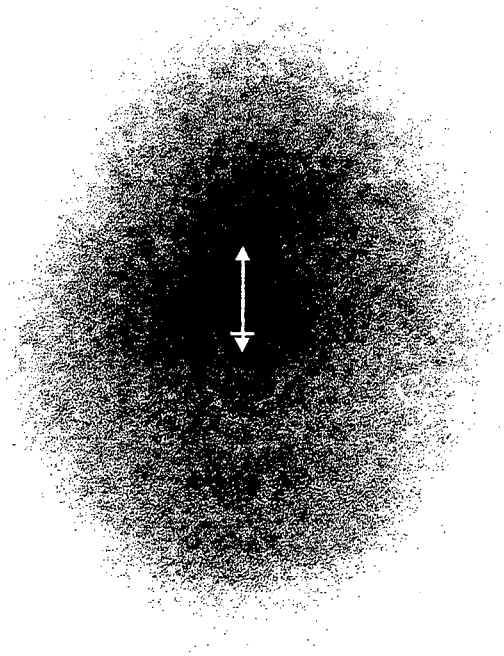

Fig. 4. AHMED et al.

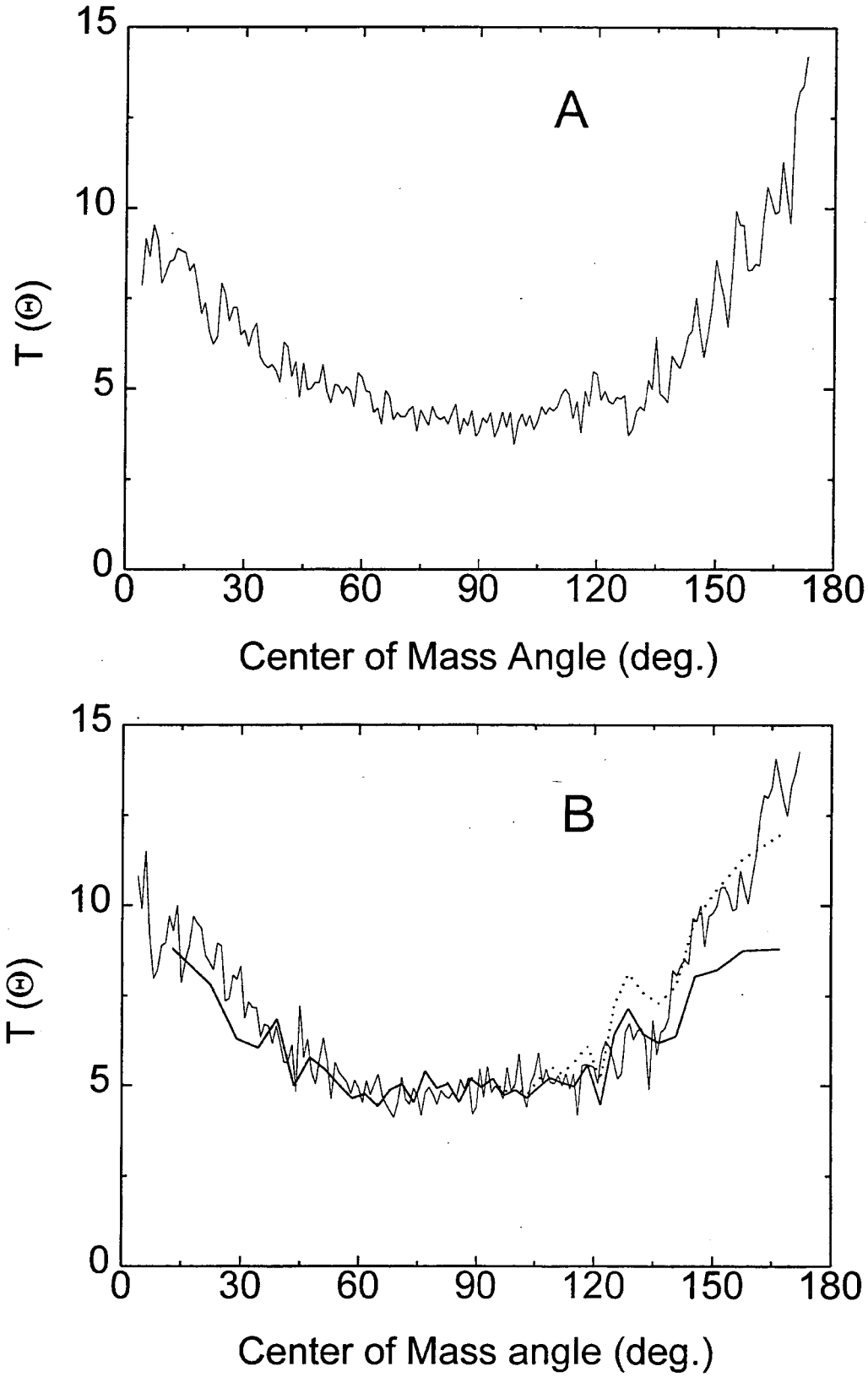

Fig. 5. AHMED et al.

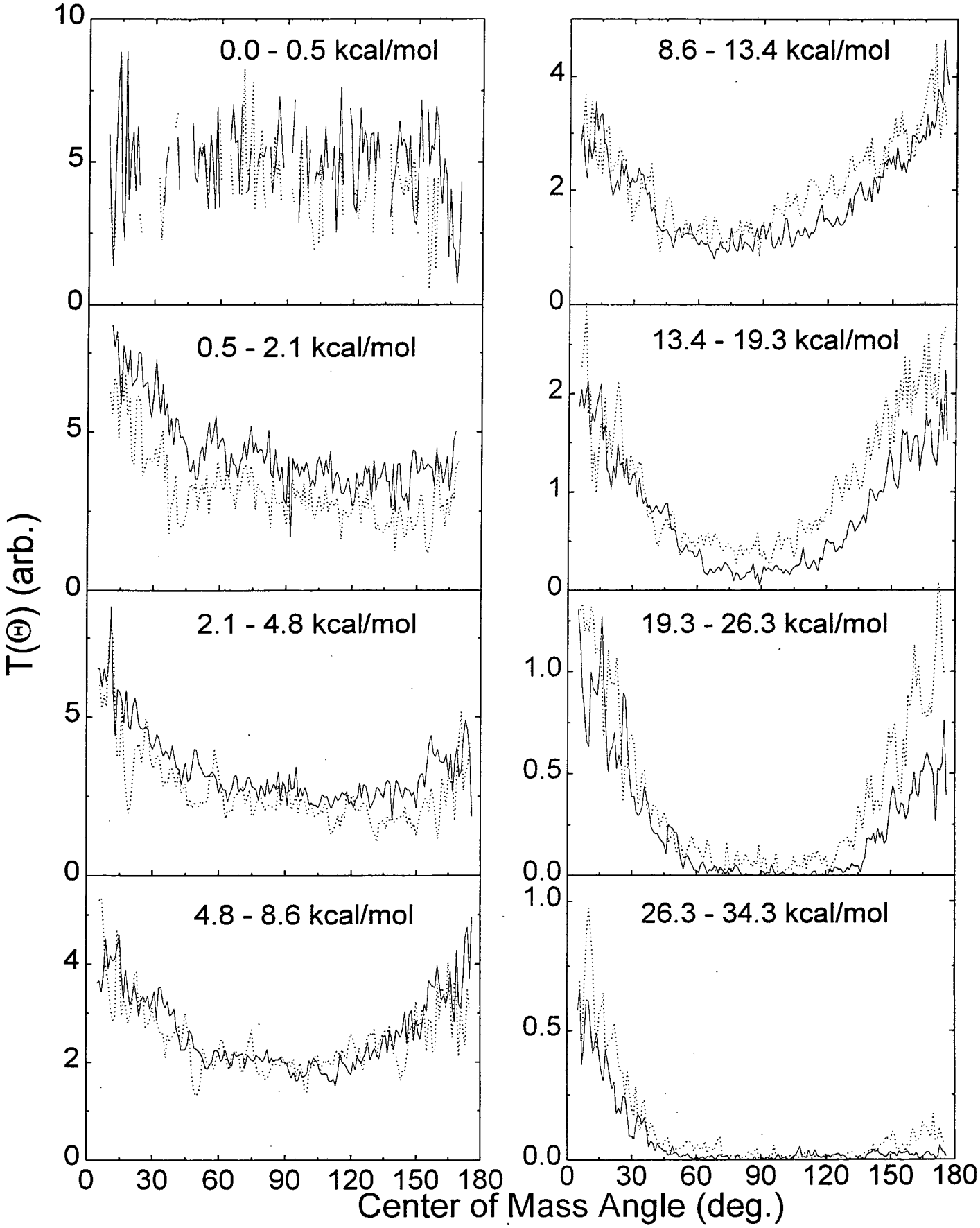

Fig 6. AHMED et al.

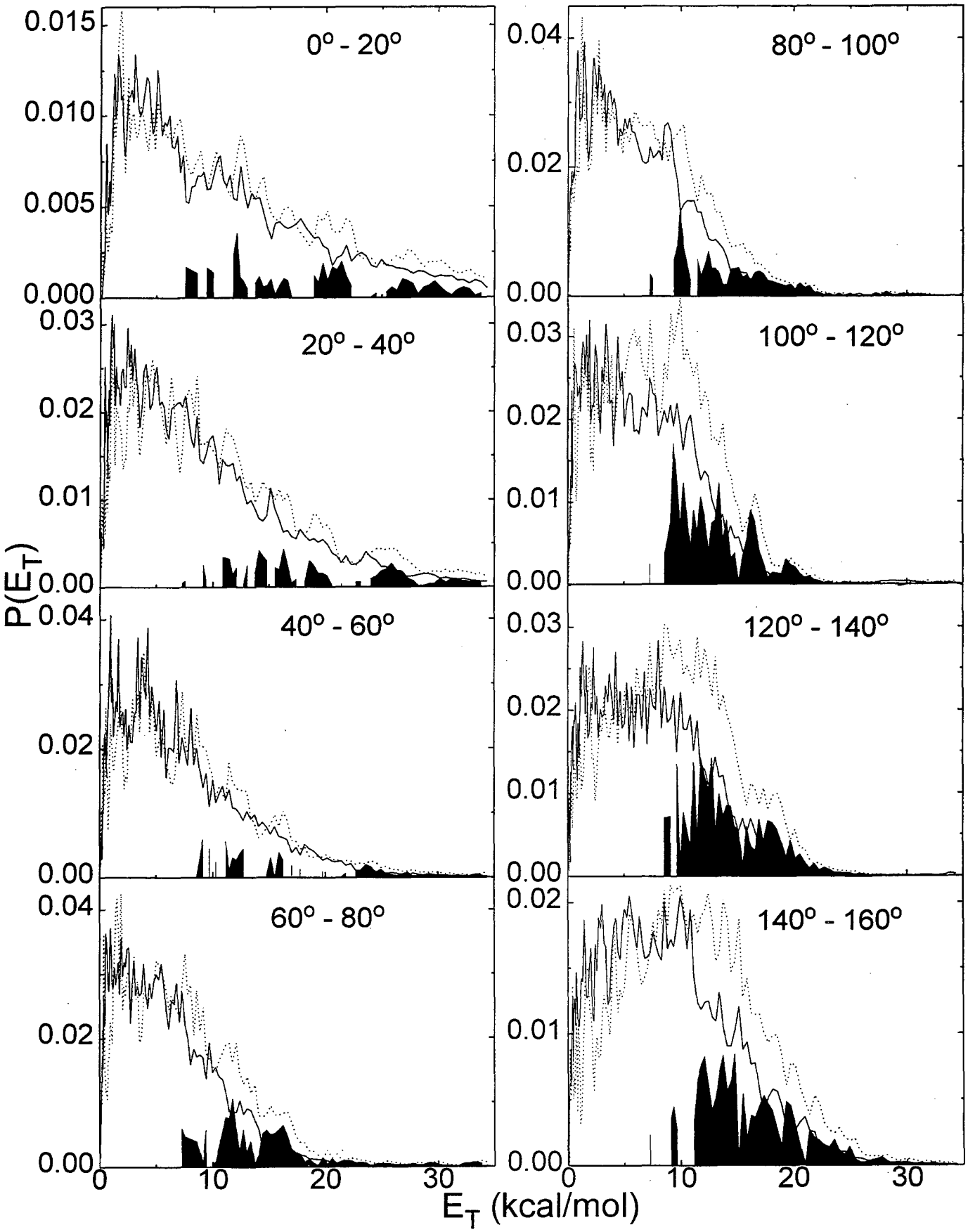

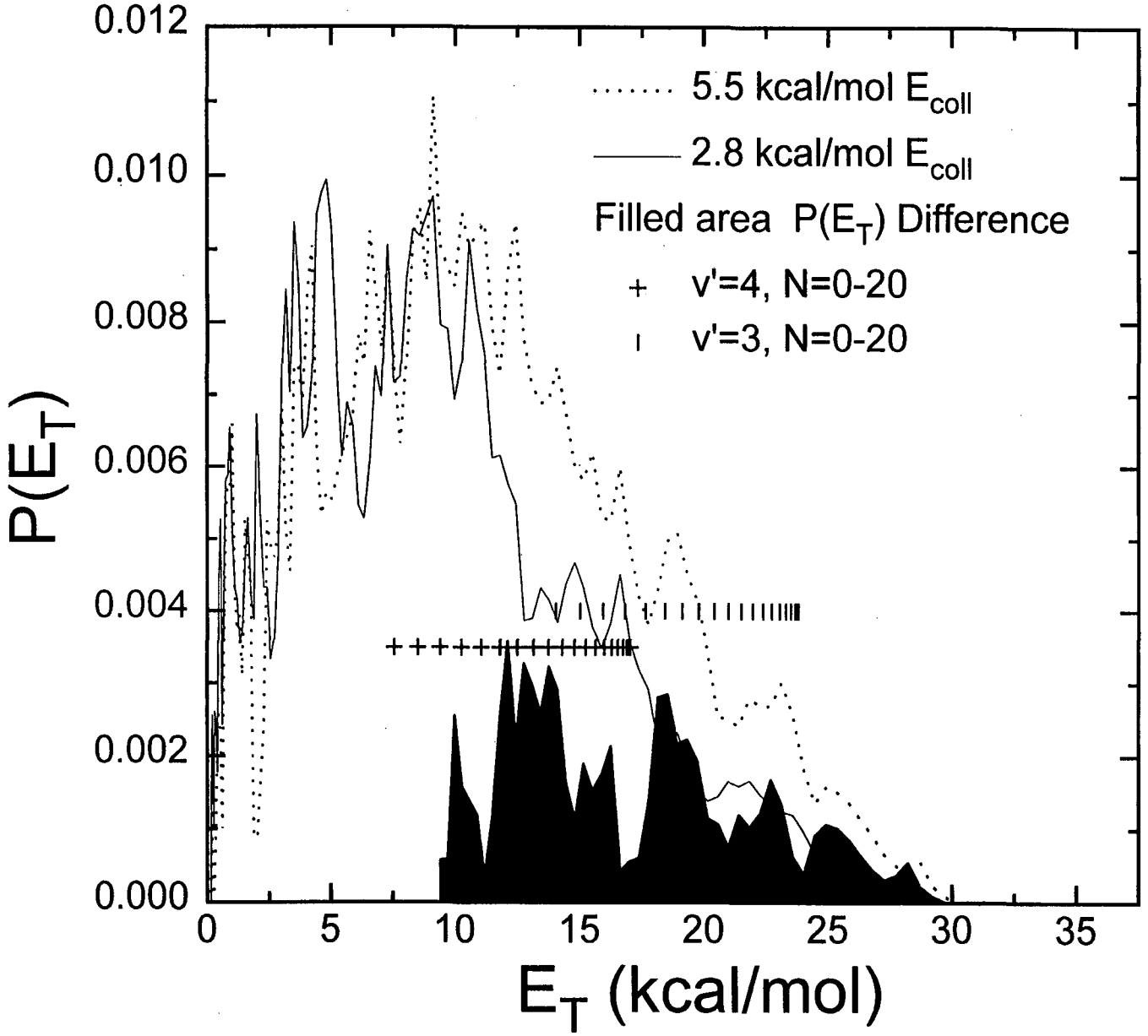

Fig. 7. AHMED et al.

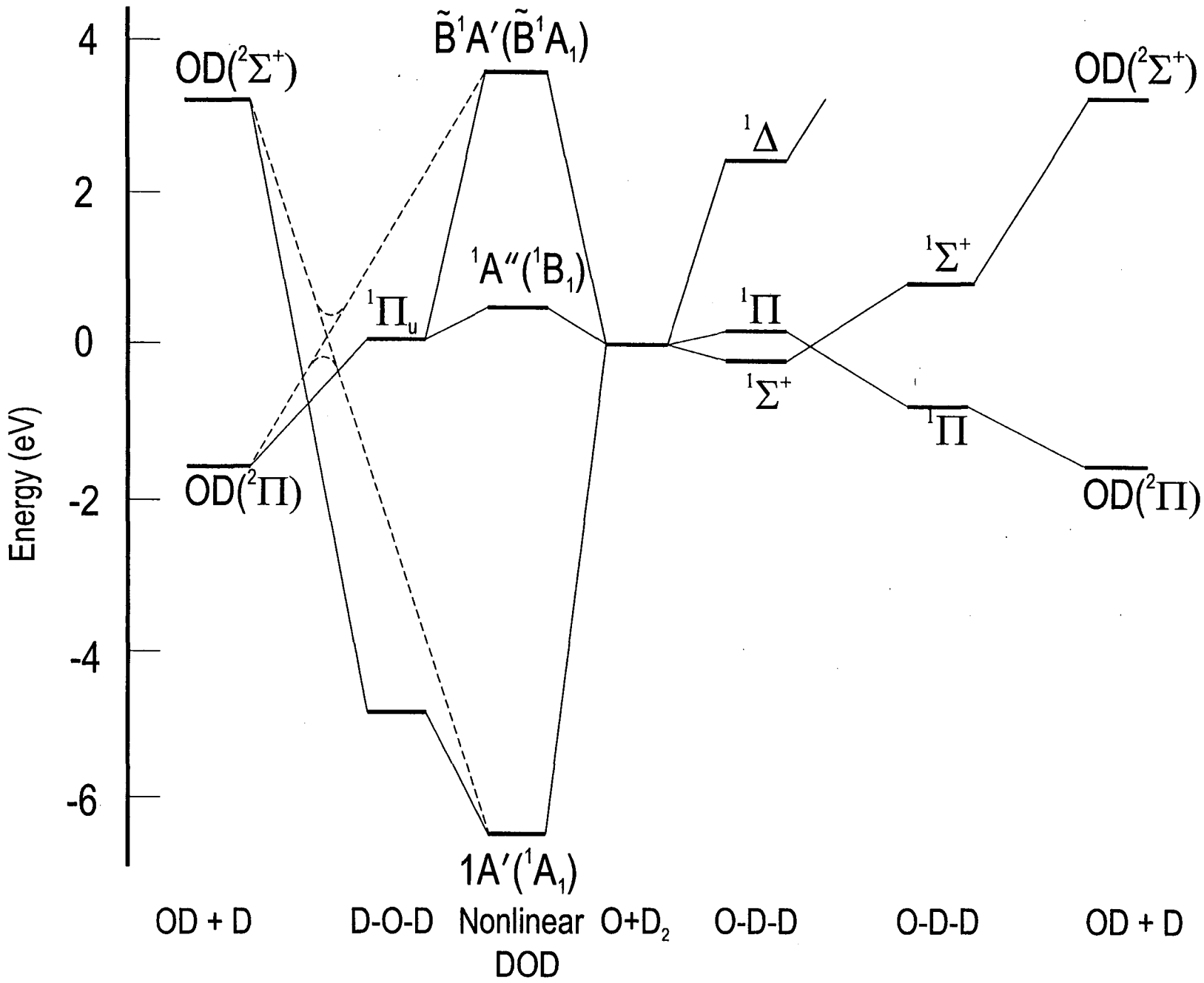

Fig 8. AHMED et al

Fig. 9. AHMED et al

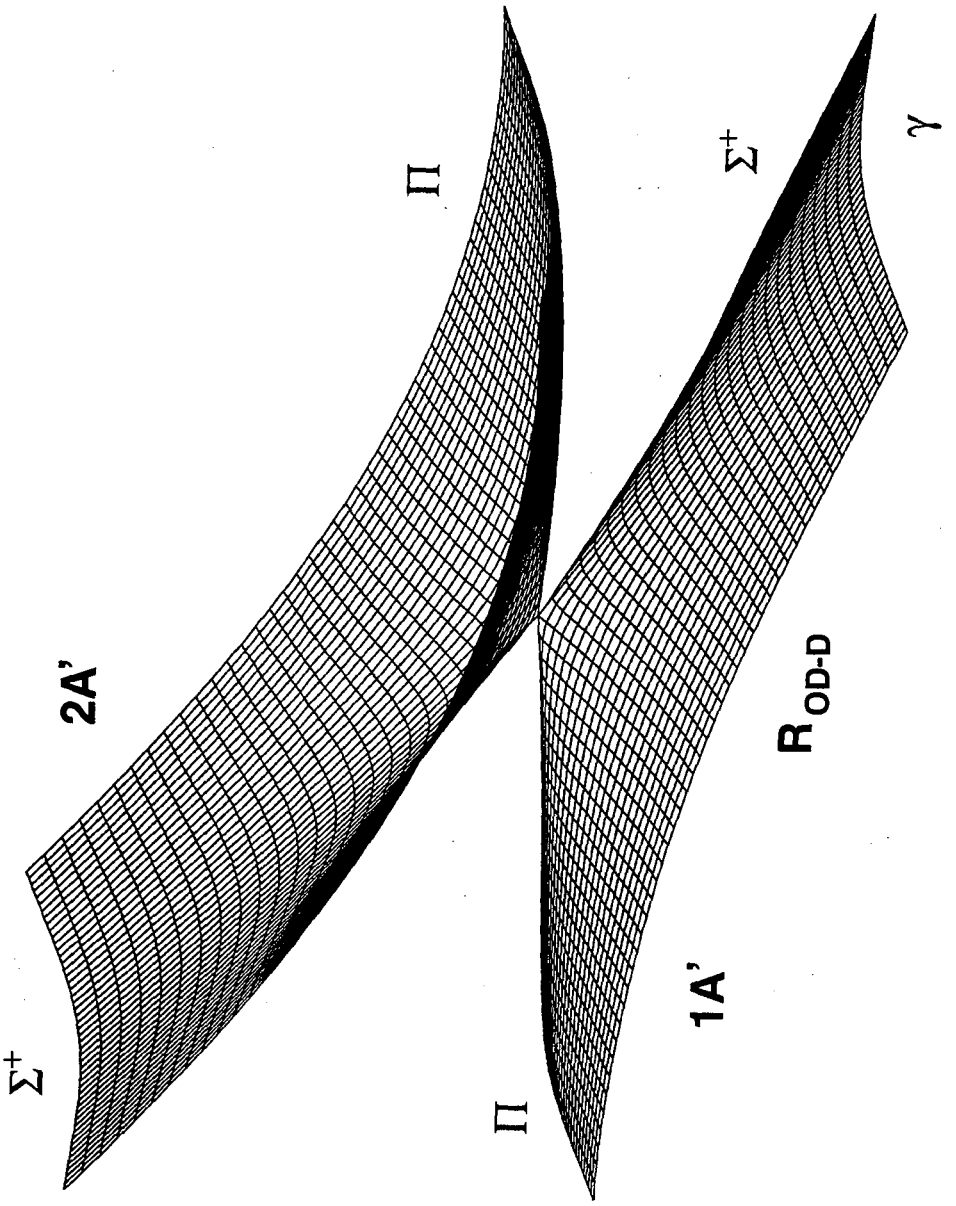

Ernest Orlando Lawrence Berkeley National Laboratory
One Cyclotron Road | Berkeley, California 94720

Prepared for the U.S. Department of Energy under Contract No. DE-AC03-76SF00098